Seismic Noise Autocorrelations on Mars

Martin Schimmel 1 , Eleonore Stutzmann 2 , Philippe Lognonné 2 , Nicolas Compaire 4 , Paul Davis 5 , Melanie Drilleau 4 , Raphael Garcia 4 , Doyeon Kim 6 , Brigitte Knapmeyer-Endrun 7 , Vedran Lekic 6 , Ludovic Margerin 8 , Mark Panning 9 , Nicholas Schmerr 6 , John Robert Scholz 10 , Aymeric Spiga 11,12 , Benoit Tauzin 13 , Bruce Banerdt 3

1 Geosciences Barcelona - CSIC, Barcelona, Spain.

2 Université de Paris, Institut de Physique du Globe de Paris, CNRS, Paris, France.

3 Jet Propulsion Laboratory, California Institute of Technology, Pasadena, CA, USA.

4 Institut Supérieur de l'Aéronautique et de l'Espace SUPAERO, Toulouse, France.

5 Department of Earth, Planetary, and Space Sciences, University of California, Los Angeles, USA.

6 University of Maryland, College Park, Department of Geology, USA.

7 Bensberg Observatory, University of Cologne, Bergisch Gladbach, Germany.

8 Institut de Recherche en Astrophysique et Planétologie, Université Toulouse III Paul Sabatier, CNRS, CNES, Toulouse, France.

9 Jet Propulsion Laboratory, California Institute of Technology; Pasadena, USA.

10 Max Planck Institute for Solar System Research, Göttingen, Germany.

11 Laboratoire de Météorologie Dynamique/IPSL, Sorbonne Université, CNRS, Ecole Normale Supérieure, PSL Research University, Ecole Polytechnique, Paris, France.

12 Institut Universitaire de France, Paris

13 Université de Lyon, Université Claude Bernard Lyon 1, ENS, CNRS, Laboratoire de Géologie de Lyon : Terre, Planétes, Environnement, Villeurbanne, France.

Contents of this file

Introduction

This Supporting Material Section contains some additional figures to strengthen our analysis of the main paper. Among others, we include figures obtained with an alternative data processing, e.g., using linear rather than non-linear stacking of autocorrelations, to further show the robustness of the identified signals. We refer to all figures in the main text of the publication, where we also describe the corresponding methods and details of the figure.
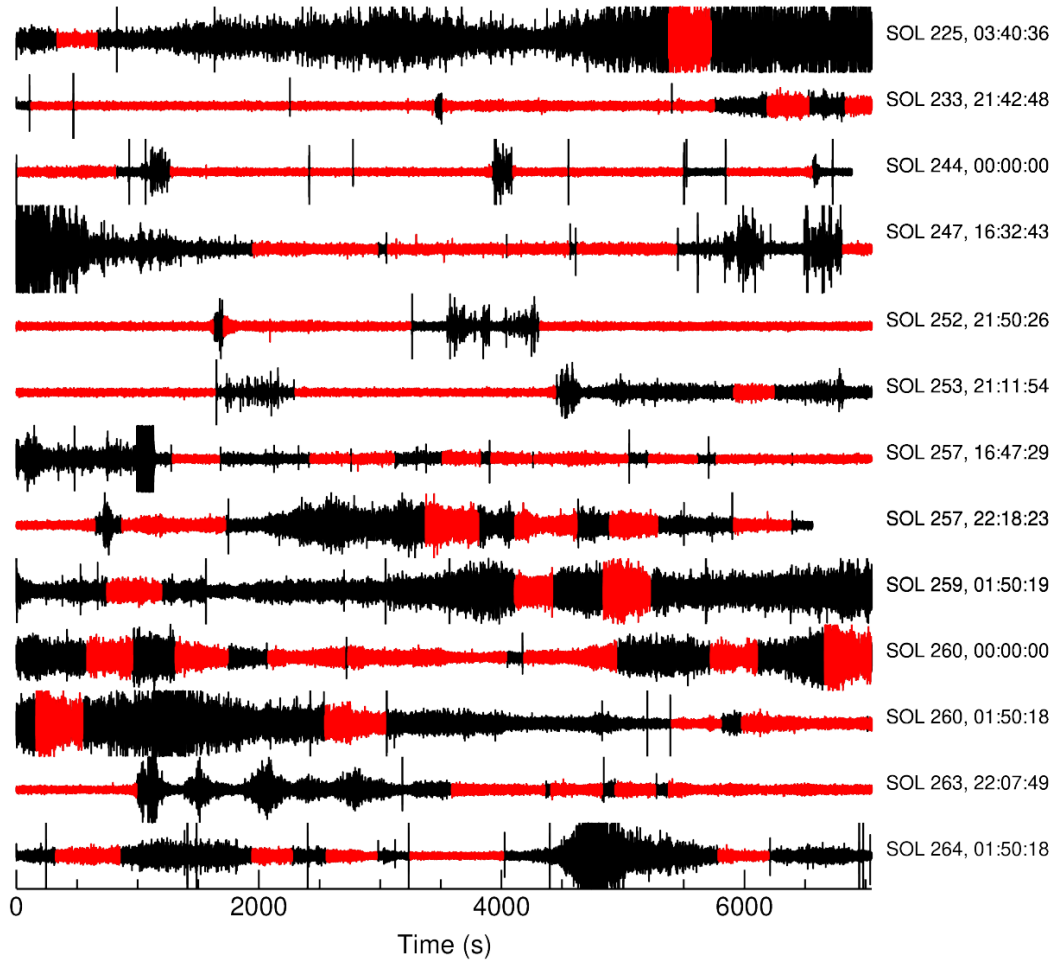
Supporting Figures S1-S9:

Figure S1. Data selection and segmentation examples. The selected segments are marked in red. The start time of each trace is given in LMST to the right of each record.
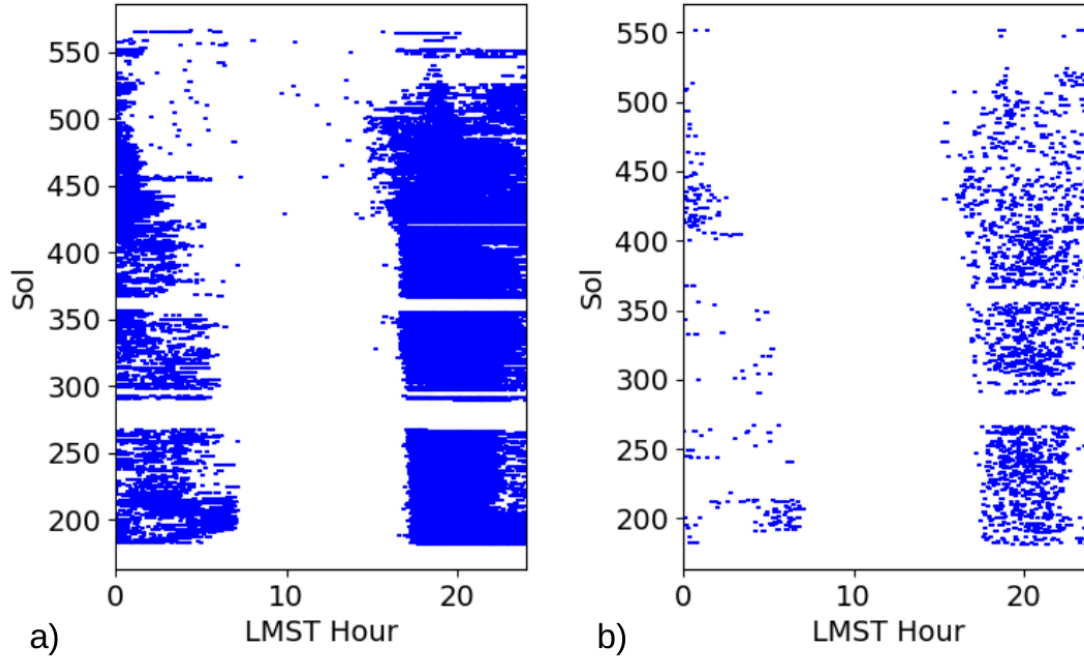
Figure S2. Selected data windows as function of Sol and LMST for the 30% (a) and 3% (b) subsidiary data sets. Very short time windows are not well resolved. Nevertheless, this figure shows that most of the selected time segments with low RMS variability are from the evening when wind activity is low.
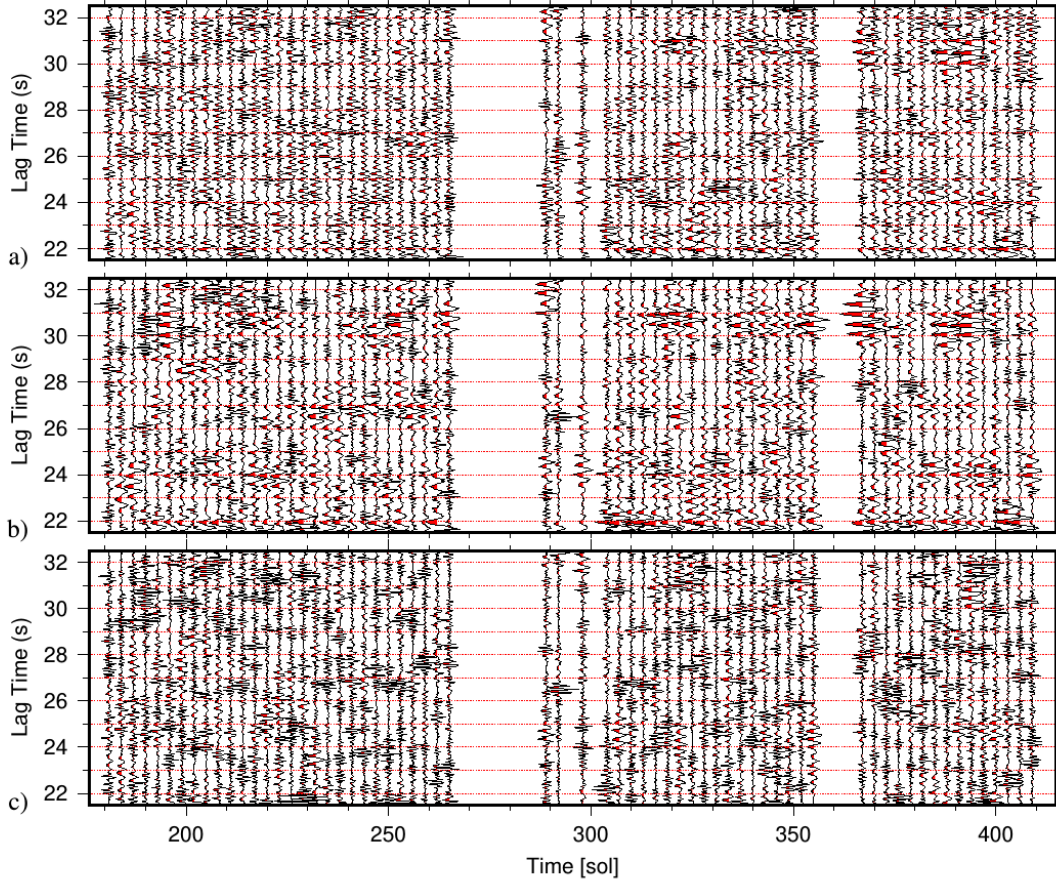
Figure S3. Same as Fig. 5, but using tf-PWS and the 3 % data set rather than the linear stack and the 100 % data set: a) Vertical-component noise autocorrelation stacks (tf-PWS) for sliding 3-Sol data windows. The frequency band is 1.2-8.9 Hz, data windows do not overlap, and positive amplitudes are in red. Phase autocorrelations are for a subsidiary data set of about 3% of the total data volume, i.e., containing the traces with the lowest RMS amplitude variability. The lag time window is large to avoid reflections from shallow discontinuities. The tick noise are the positive amplitude signals at every full second. b) Same as a), but two band-rejection filters, 3.9-4.4 Hz and 6.8-7.2 Hz have been applied before computation of the phase autocorrelations. c) Same as b), but the data has been filtered with a third band rejection filter 1.9-2.5 Hz.
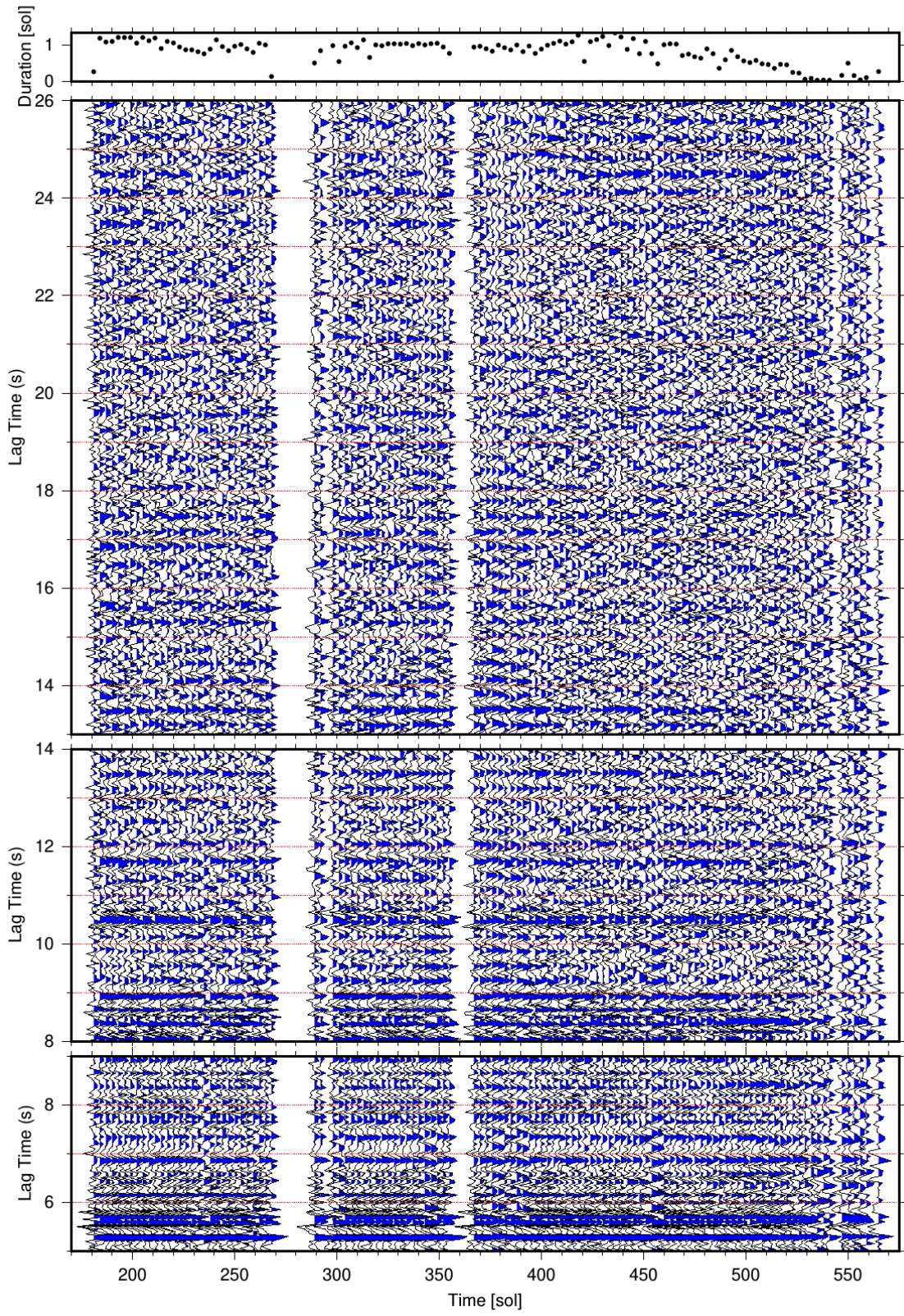
Figure S4. Same as Fig. 9, but employing the linear stack rather than the tf-PWS: Vertical-component noise autocorrelation stacks for sliding 30-Sol data windows. The frequency band is 1.2-8.9 Hz and data windows do not overlap. Shown are linear stacks of phase autocorrelations. Blue marks negative amplitudes. The three lag-time windows have been used to improve the visibility through independent amplitude normalization. The top panel shows the total duration of the selected data used to compute autocorrelations within each of the 30-Sol data windows. The axis for the duration of the 30 % and 3 % data set are scaled by the number to the top left.
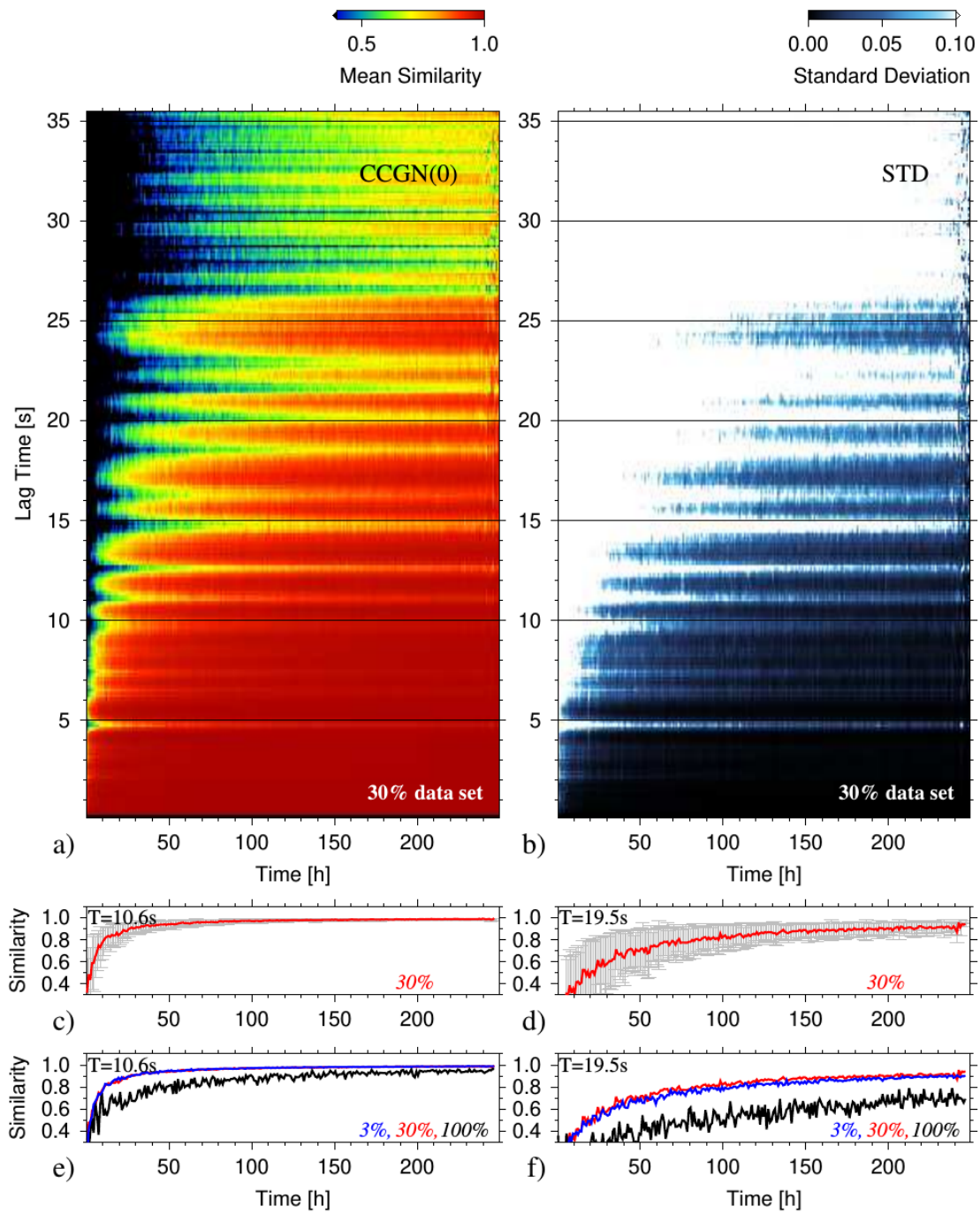
Figure S5. Same as Fig. 8, but using zero-lag CCGN rather than PCC to measure the waveform similarity. Note that the autocorrelations have been computed with PCC. In comparison to Fig. 8, this figure shows an apparent faster waveform convergence as PCC is the more sensitive approach to measure waveform similarity.
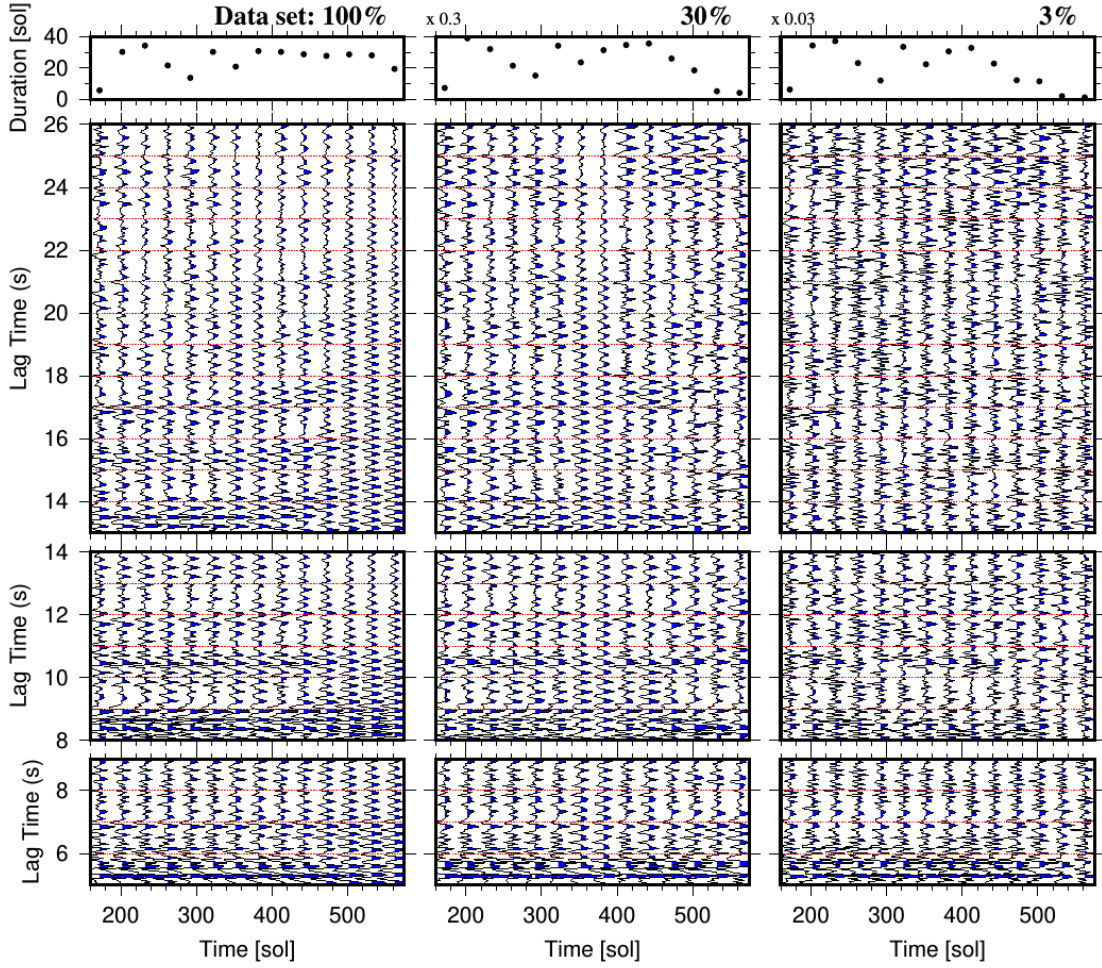
Figure S6. Same as Fig. 9, but employing the linear stack rather than tf-PWS: Vertical-component noise autocorrelation stacks for sliding 30-Sol data windows. The frequency band is 1.2-8.9 Hz and data windows do not overlap. Shown are linear stacks of phase autocorrelations. Blue marks negative amplitudes. The three lag-time windows have been used to improve the visibility through independent amplitude normalization. The top panel shows the total duration of the selected data used to compute autocorrelations within each of the 30-Sol data windows. The axis for the duration of the 30 % and 3 % data set are scaled by the number to the top left.
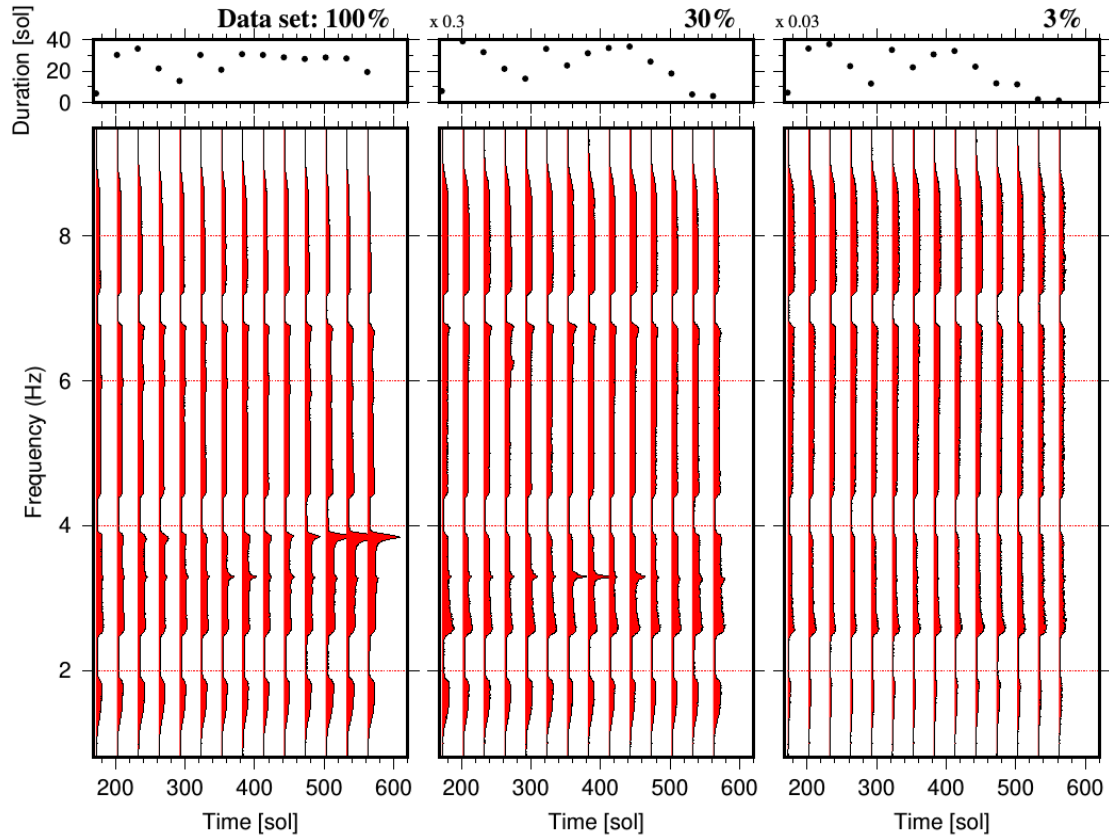
Figure S7. Same as Fig. 10, but using linear stacks: Amplitude spectra of linearly stacked autocorrelations as function of Sol for the 100 % (left panel), 30 % (middle panel), and 3 % (right panel) data sets. Stacks are build using all available autocorrelations within non-overlapping 30-Sol data windows. Each amplitude spectrum is placed at its window center time and has been normalized at 6 Hz. The total duration of data used to compute the autocorrelations within each 30-Sol window is plotted to the top. The numbers to the top left are factors to reduce the duration axes of the 30 % and 3 % data sets.
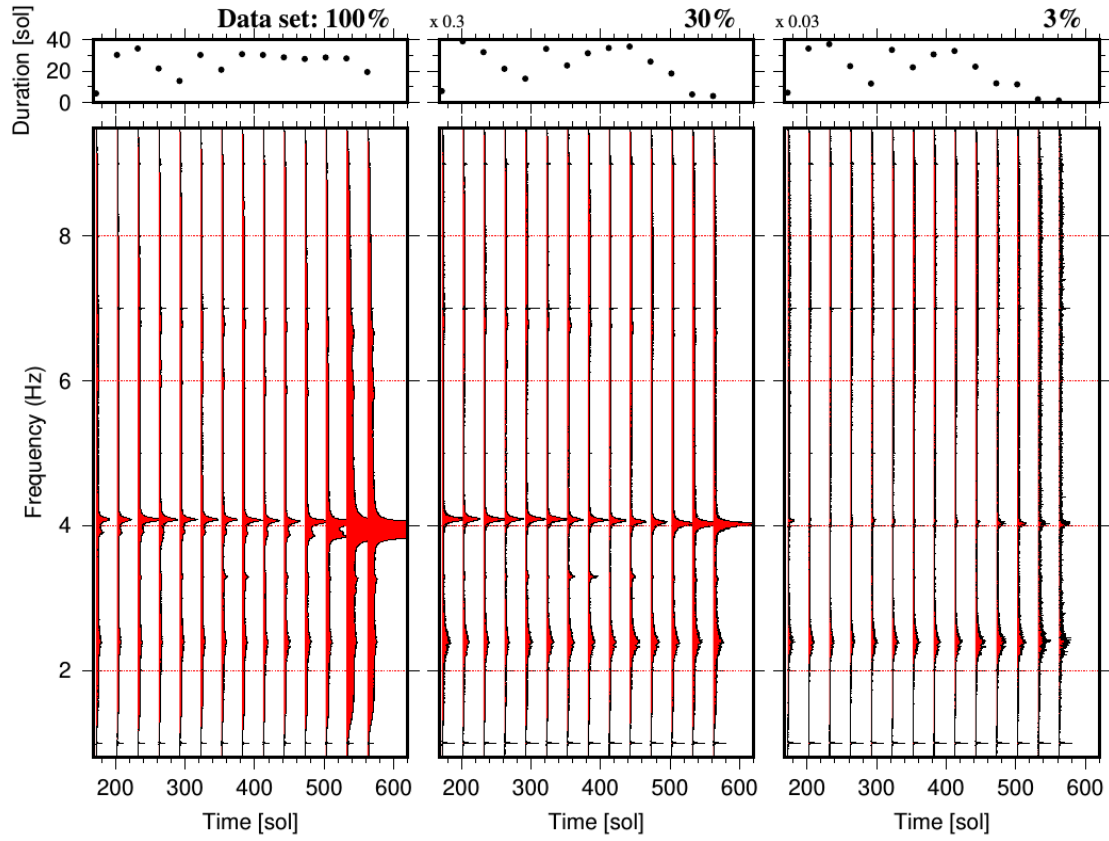
Figure S8. Same as Fig. S7, but using a slightly broader frequency band (0.8-9.5 Hz) and no band-rejection filters. Spectra are normalized at 1 Hz and amplitudes have been multiplied by 0.5 for the 100 % data set (left panel).
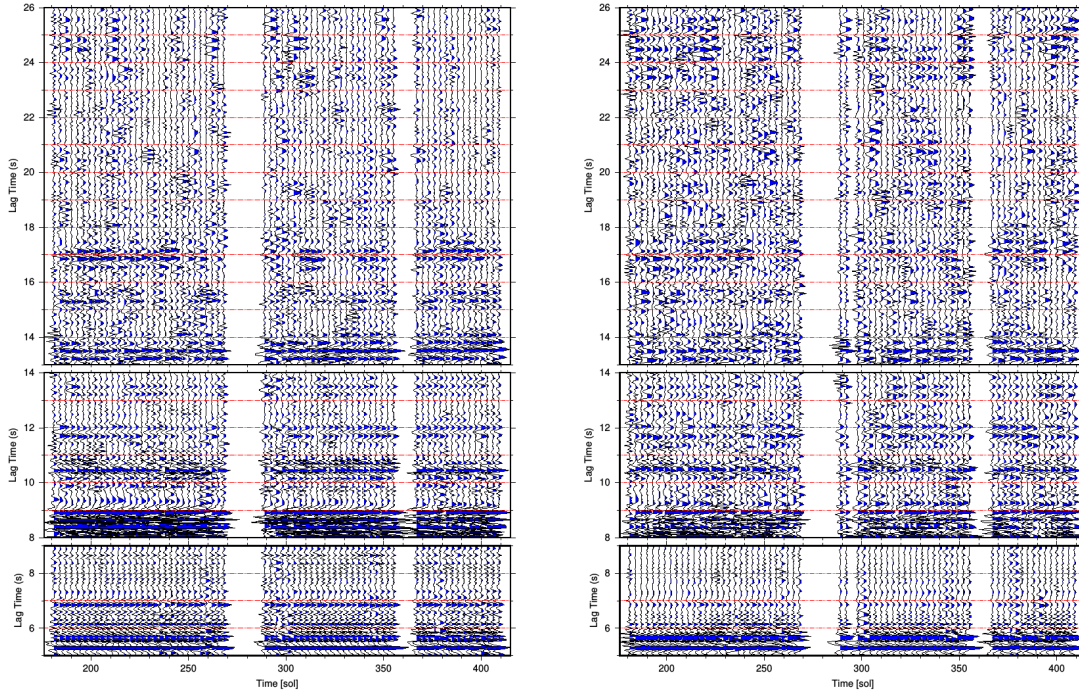
Figure S9. Vertical-component autocorrelation stacks for sliding 3-Sol data windows. The frequency band is 1.2-8.9 Hz and data windows do not overlap. Shown are tf-PWSs of phase autocorrelations computed for the 100 % (left panel) and 30 % data set up to Sol 410. Most of the signals appear for both data sets. This further testifies that PCC is a robust approach as data problems, glitches and donks present in the 100 % data set do not bury the signals shown with the 30 % data set.